Available online at www.sciencedirect.com

ScienceDirect

journal homepage: www.elsevier.com/locate/he

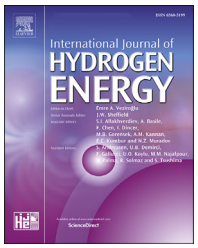

Degradation analysis of commercial interconnect materials for solid oxide fuel cells in stacks operated up to 18000 hours

Manuel Bianco [a,*], *Jan Pieter Ouweltjes* [b], *Jan Van herle* [a]

[a] *Group of Energy Materials, Inst. Mech. Eng., Ecole Polytechnique Fédérale de Lausanne (EPFL) Valais, CH-1951, Sion, Switzerland*

[b] *SOLIDpower SA, CH-1400, Yverdon-les-Bains, Switzerland*

HIGHLIGHTS

- The stack survives the degradation caused by perovskite/interconnect interaction.
- The degradation at the air side of the interconnect stabilizes after 5000 h.
- The tested SOFC stack is robust: it can withstand more than 120 thermal cycles.
- The results partially disaffirm the reliability of ex-situ tests on interconnects.

ARTICLE INFO

Article history:
Received 31 July 2019
Received in revised form
26 September 2019
Accepted 30 September 2019
Available online 25 October 2019

Keywords:
SOFC stack
Interconnects
Protective coating
Corrosion
Lifetime degradation
Ferritic stainless steel

ABSTRACT

Despite being a mature technology, solid oxide fuel cell (SOFC) devices are still limited by lifetime issues. In SOFC stacks, cell/interconnect interaction is the main responsible for voltage degradation at the oxygen electrode side. Corrosion and chromium evaporation might in fact increase ohmic and charge transfer losses. This study presents the evolution of the degradation phenomena inside four SOFC short-stacks tested respectively for 45, 2700, 4800 and 10000 hours. An additional stack which underwent 124 thermal cycles is also analyzed to assess the mechanical reliability of the interconnect/ceramic coupling. Metal interconnect was made of K41/AISI441 ferritic stainless steel coated with $MnCo_2O_4$ porous barrier layer. Scanning electron microscope (SEM) coupled with energy dispersive X-ray spectroscopy (EDS) characterization is applied to examine the degradation process. Observations indicate that despite a harsh initial red-ox interaction between the cathode materials and the interconnect, after 5000 h of operation the kinetic of the degradation process in the electrical contact areas slows down dramatically. An empirical model based on the scale thickness at different interconnect location gives estimation for the oxide thermal growth for a stack lifetime period. From the mechanical properties point of view, no spallation was observed and local delamination was mainly due to the sample preparation process.

* *Corresponding author.*
E-mail addresses: manuel.bianco@epfl.ch, manuel.bianco.pro@gmail.com (M. Bianco).

https://doi.org/10.1016/j.ijhydene.2019.09.218

Introduction

In the contribution to clean and more efficient energy conversion to reduce CO_2 and polluting emissions, solid oxide fuel cell (SOFC) electrochemical devices transform chemical energy from fuel + air directly into electric power with high efficiency and negligible emissions of NOx and other pollutants [1]. Ceramic cells are stacked in series to add up voltage and obtain useful power outputs. In planar designs, each cell pair is separated by an interconnect plate in order to separate air from fuel, collect the electrical current and ensure mechanical stability [2]. In the first generation of SOFCs stacks based on electrolyte supported cells operating at rather high temperature (>850 °C), the interconnects were made of ceramic materials, with relatively low chemical inertia but high cost and limited mechanical properties. With the reduction of the electrolyte thickness achieved by transferring the mechanical support function to an electrode (typically the anode), the stack operating temperature could be decreased (<800 °C) and iron metal based interconnects introduced. Nowadays, the state of the art material is ferritic stainless steel (FSS) which provides a reasonable coefficient of thermal expansion (CTE) match with the cell ceramics and good mechanical strength at the stack operating conditions. Specific ferritic stainless steels like Crofer 22 APU/H [3] or Sanergy HT have been produced for use in SOFCs, yet their still relatively high cost made standard commercial K41/AISI441 FSS an attractive alternative.

During its use in a SOFC stack, the metallic interconnect (MIC) interacts with agents such as oxygen, steam, sealing materials and cell materials at high temperature and as such is subjected to harsher lifetime issues compared to common FSS applications.

To evaluate the reliability of this material for SOFC application, K41/AISI441 has been exhaustively characterized *ex situ:* in dual atmosphere conditions [4], coated with perovskites [5], coated with spinels [6] and tested uncoated as well [7]. Nevertheless, such studies are not fully representative of the use in a real stack; laboratory conditions usually focus on a few precise parameters, rarely considering all interactions within a stack. At the moment, the main technical limit for SOFC commercialization is long-term reliability of the stack components and the high costs of the materials used, hence assessment of the behaviour of the materials in real operating conditions is a necessary step. The present paper reduces the gap between laboratory research and field application assessing the chemical and mechanical reliability of K41/AISI441 as metal interconnect on the long term. This is important for the SOFC practitioners because substituting Crofer 22 APU or H with the commercial steel grade K41/AISI441 could significantly decrease the stack manufacturing cost [8]. In other words, substituting specific, but expensive, materials with commercial alternatives would help SOFC commercialization, but it is first necessary to demonstrate the durability of the alternative material solutions. For a readership of SOFC manufacturers and experimental researchers this information is of interest because it will help to orient future tests.

This study is necessary because so far, few studies disclosed detailed microstructural information of stacks operated for extended runs. The Research Centre Jülich reported insights on the behaviour of atmospheric plasma spray coated Crofer 22 APU up to 35000 h of operation [9], Chou et al. studied the behaviour of Ce-(MnCo) spinel coated AISI 441 in a 3-cell stack run for 6000 h [10] and Hexis partially disclosed results on a stack run for 40000 h [11]. Another recent article partially disclosed the microstructural behaviour of commercial steel grade SUS430 tested in a 10 SRUs stack, however the lack of a coating on the interconnect, together with the short operational time of 700 h does not provide useful information for practical application [12]. The same group presented also a post-test analysis on a 5-cells stack, but it was run for just 250 h [13].

The absence of a complete degradation story of the stack is a lack of these analyses, as they describe the situation typically for one case. To give a whole representation of the degradation process, it is instead necessary to observe the stack for different operation durations, including the initial one.

This work adds a contribution to these aspects, through an unprecedented analysis of SOFC stacks tested for 45, 2700, 4800, 10000 and 18000 h. A history of degradation observed on K41/AISI441 $(MnCo)_3O_4$ coated MICs is presented, with particular emphasis given to the interaction between the MIC and the cell ceramics at the cathode side. At the oxygen electrode side, interaction between the interconnect and the cell materials is intense, notably the chromium from the steel substrate reacting with the perovskite materials of the cathode cell. The formation of $SrCrO_4$ for example is a known limiting phenomenon for stacks lifetime [14,15]. At the fuel electrode side instead, the reaction between the cell and interconnect materials presents no critical issues for the stack. Nevertheless, the oxide growth at the MIC side exposed to the fuel environment will also be presented, as the oxide thickness influences the ohmic losses and therefore the voltage degradation of the stack. This section will be important also for a more theoretical readership, the data provided are a novel sources of validation for researchers modelling the stack behaviour. The harmful phenomena affecting the MIC's steel lifetime will be identified and discussed, both from the corrosion and mechanical point of view. Moreover, a forecast on overall degradation will be given.

Materials and experiments

Six prototype short stacks tested for different durations are presented in this work. Each stack was provided by SOLIDPower S.p.A. (SP). One of these stacks has been tested to assess thermal cycling resistance, while the others were operated under steady state conditions. The labelling and run time conditions of each stack were as follows:

- #45: 6-cell stack, 45 h operation at 720–780 °C, I–V characterized;
- #2700: 66-cell stack, 2700 h operation at 720 °C, 0.3 Acm^{-2} current density;
- #4800: 6-cell stack, 4800 h operation at 720–780 °C, 0.4 Acm^{-2} current density;

- #10000: 6-cell stack, 10000 h operation at 720–780 °C, 0.4 Acm^{-2} current density;
- #18000: 2-cell stack, 18000 h operation at 720–780 °C, 0.25 Acm^{-2} first 12000 h and 0.05 Acm^{-2} up to 18000 h
- #124 TC: 6-cell stack, 2600 h operation, 124 thermal cycles between 25 °C and 750 °C, 0.4 Acm^{-2} current density.

In all cases, feed gases were air at the cathode with low oxygen utilization (10% in nominal condition), and N_2/H_2 mixture at the fuel side. Manufacturing and other operational details are SP proprietary information.

The analysed sample cross sections come from systems with the aim of simulating real operation conditions, hence they were not all tested under identical conditions. Stack #2700 was run at a lower temperature than the other stacks. This difference affects the kinetics of the corrosion process but not the final products, still allowing for qualitative comparisons. Stack #18000 underwent the last 6000 h of operation at low current density to limit cell degradation, but this is not critical for the discussion as it will be shown that degradation processes in MICs tend to stabilize.

The paper reports the representative average of the observed behaviours, and not the specificity of each stack and region of interest.

The MICs are K41/AISI441 steel plates (Table 1) coated by a protective $MnCo_2O_4$ (MCO) spinel layer deposited by wet powder spraying (WPS) and then heat-treated to densify it. The coating composition and deposition technique are used by the industrial manufacturer for competitive cost reasons. The coating, even when initially porous after the deposition process, serves to lower the chromia scale growth rate and the release of volatile chromium compounds. The cells were Ni-YSZ porous anodes supporting an yttria-stabilized zirconia (YSZ) electrolyte followed by a gadolinium doped ceria (GDC) barrier layer, and finally a $LaSrCoFeO_3$ (LSCF)-GDC composite cathode.

After the completion of each test, the stack was disassembled from the test bench and each single repeating unit (SRU) removed one by one. For each stack, one SRU, chosen after visual inspection, was embedded in Struers speciFix 20 epoxy resin. With a diamond-coated disk saw, cross-sections of about 2*5*5 cm^3 were extracted from the embedded block. The sections were polished with SiC paper up to 1200 fine grit size and then finished with 6, 3, and 1 μm diamond paste.

The polished cross-sections received a carbon coating and were analysed by FEI's TENEO Scanning Electron Microscope (SEM) coupled with Bruker's Energy Dispersive X-Ray Spectrometer (EDS).

Data obtained were post-processed with ImageJ and the computational software MathWorks' Matlab. For each interface of each stack, at least six different regions of interest were analysed.

Table 1 – Average composition of the MIC steel substrate (wt.%) [16].

Steel	Fe	Cr	Si	Nb+Ti	Mn	C	N
K41/AISI441	Bal.	17.7	0.6	0.55	0.25	0.02	0.015

Results

In the analysis of the interconnects, four regions of interest (ROI) are defined based on the scientific and technological relevance (Fig. 1):

1) "cathode side rib" (oxidizing atmosphere, direct electrical contact with the cell, MIC is coated);
2) "cathode side valley" (oxidizing atmosphere, not in electrical contact with the cell, MIC is coated);
3) "dual exposure cathode side" (oxidizing atmosphere, not in electrical contact with the cell, MIC is uncoated);
4) "dual exposure anode side" (reducing atmosphere, not in electrical contact with the cell, MIC is uncoated).

In Fig. 1 the fluted regions at the left and right ends of the picture indicate that this sketch is just a portion of the interconnect and of the cell. In reality, the left and right edges of the interconnect are closed, therefore the air lapping the uncoated side of the interconnect sheet never encounters the cells.

Cathode side rib

In this region, the coated MIC is in direct contact with the cathode perovskite material. Besides the temperature, mechanical stresses, and polarization contribute to material evolution. Consequently, this interface underwent most of the changes observed in the stacks.

Fig. 2 gives the time evolution of this interface composed of steel/oxides/MCO/perovskite for five of the investigated stacks. A representative observation for each operating time is given. Note that among the different layers some void regions containing resin (black zones) appear; these originate from disassembling the stacks. Colours are superimposed to the pictures in Fig. 2 to identify the evolution of the different layers. All the corrosion products are *oxides* or *scales* and indicated with green colour; blue colour represents the MCO *densified coating* by sintering and, mainly, iron incursion; the reaction product $SrCrO_4$ is associated to dark red; chromium-poisoned perovskite, finally, is coloured with light red. Fig. 3 displays the EDS chemical mapping of interfaces similar to those in Fig. 2, but in different regions of interest.

After 45 h, isolated elliptical regions were discretely distributed along the steel/MCO interface (Fig. 2 top left). The hemisphere top is radially spreading into the MCO coating, densifying it; while the bottom half proceeds via inward corrosion - this behaviour is comparable with Fe breakaway corrosion [17]. Where these bump-like protrusions are not present, the scale is thin and regular; at the interface with MCO a thin dense oxide layer is formed. In Figure 2 and 45 h, this condition is at the left and right of the inward corrosion area.

The densification of the first microns of porous MCO protective coating in contact with the thermally grown oxide is a known phenomenon [18]. The scale composition is not homogeneous along the interface: when standard corrosion is observed, it is made of discontinuous SiO_2 and TiO_2 [19] attached to a bulk $Cr_2O_3/(MnCr)_3O_4$ double layer. In case of

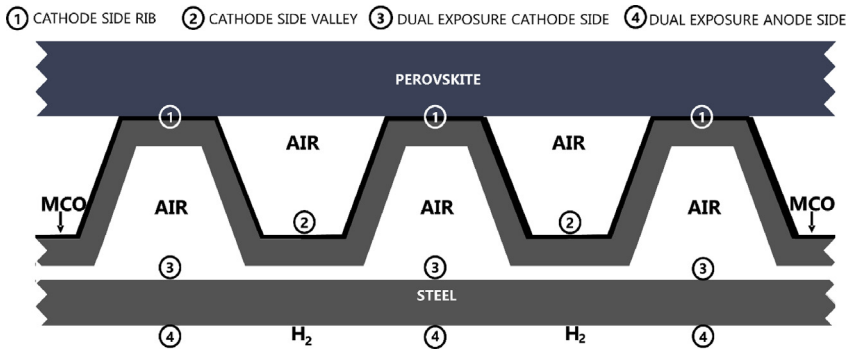

Fig. 1 – Schematic not-to-scale representation of the interconnect in contact with the perovskite and the four distinct regions of relevance.

inward corrosion instead, the scale composition is not stoichiometrically defined among Cr, Fe, Mn and O.

In the #45 h stack, dense precipitations appear between the MCO protective coating and the perovskite material. EDS analysis revealed a Sr:Cr ratio close to 1, suggesting $SrCrO_4$ formation (dark red in Fig. 3–45 h). Some of these aggregates are observed also inside the MCO coating in stack #45. Strontium traces are found in proximity of the oxide too, but due to the small amount these traces are not visible in Fig. 2–45h and Fig. 3–45 h. Please note that these traces are not represented by the strip at the steel/scale interface in the Sr map, this layer is instead due to the overlap with the Si EDS signal. The EDS peak at 14.14 keV – specific of strontium – was always checked during the analysis to be certain of the presence of strontium and not to confuse it with silicon.

At 2700 h (3.5 months) the densification of the porous coating propagated extensively (Figs. 2 and 3). The densification is present inside the entire MCO layer in direct contact with the perovskite. Chemical analysis revealed that the densified coating is mainly made of MCO infiltrated by Fe (up to 36% at.), with presence of Cr and traces of Sr at the interface with the scale. In addition, we found Si, Ti and Nb precipitates at the scale/densified coating interface indicating the original steel/scale border. Inward corrosion further progressed into the steel substrate, and the corrosion front profile became irregular with the merging of single enhanced corrosion regions.

Advancing towards 4800 h (6.5 months), 10000 h (14 months), and 18000 h (24 months) of stack operation, scale and densified coating show less morphological differences (cf. Fig. 2). In all the stacks strontium migration from the perovskite is confirmed. Figure 2 and 4800 h, presents a region of interest where $SrCrO_4$ binds the densified coating and the perovskite, this interaction being strong enough to survive the stack disassembling. Moreover, Figure 3 and 4800 h, highlights a phenomenon not observed in stack #45 and #2700: an intense steel inward corrosion with $SrCrO_4$ as likely product. This type of corrosion was found in a few regions of interest in stack #4800.

In stack #10000 strontium stopped at the interface with the scale or reacted directly with the chromium in the steel like for some regions of stack #4800 (cf. Figure 2 and 4800 h). If such regions with aggressive corrosion spots were rare to find in stack #4800, in stack #10000 they were frequently found.

A similar behaviour is observed in stack #18000 too (Fig. 3). Indeed, strontium chromate is the main corrosion product on the steel surface. The densified coating is a mixture of the original MCO and $SrCrO_4$ (Fig. 3 18000 h). Minor amounts of regions presenting Fe breakaway corrosion behaviour are seen as local spots interrupting the $SrCrO_4$ densified coating.

Apart from the strontium chromate segregates, chromium poisoned the whole perovskite zone in contact with the interconnect in all the stacks analysed (Fig. 2). The light red colours in Fig. 2 indicate chromium contamination up to 9 at. %.

K41 small coupons, coated with porous MCO and in contact with the same perovskite materials presented here, were tested also in similar conditions [20]. However, the chemical interactions between the materials were more mild. Notably, no strontium chromate or Fe breakaway were found in small samples.

The mechanical aspects of the cathode side rib interfaces up to 18000 h appear good. Randomly distributed cracks and porosities were found at the scale/densified coating in all stacks but #45. Such regions match with deposits rich in Si, Nb and Ti oxides. The crack concentration at the scale/densified coating interface of the cathode side rib region was confirmed by the post-analysis of the stack which underwent 124 thermal cycles (discussed later, cf. Fig. 7).

Cathode side valley

In this region, the coated steel is not in direct electrical contact with the perovskite.

Fig. 4 illustrates the time evolution of this region. Two different behaviours exist below and beyond 10000 h of operation. Up to 10000 h, the MCO coating densified only in the first microns close to the steel/MCO interface. SEM/EDS analysis revealed traces only of Fe diffusion inside the protective coating.

The oxide layer has grown smoothly all along the steel/MCO interface in all the observed samples, its composition

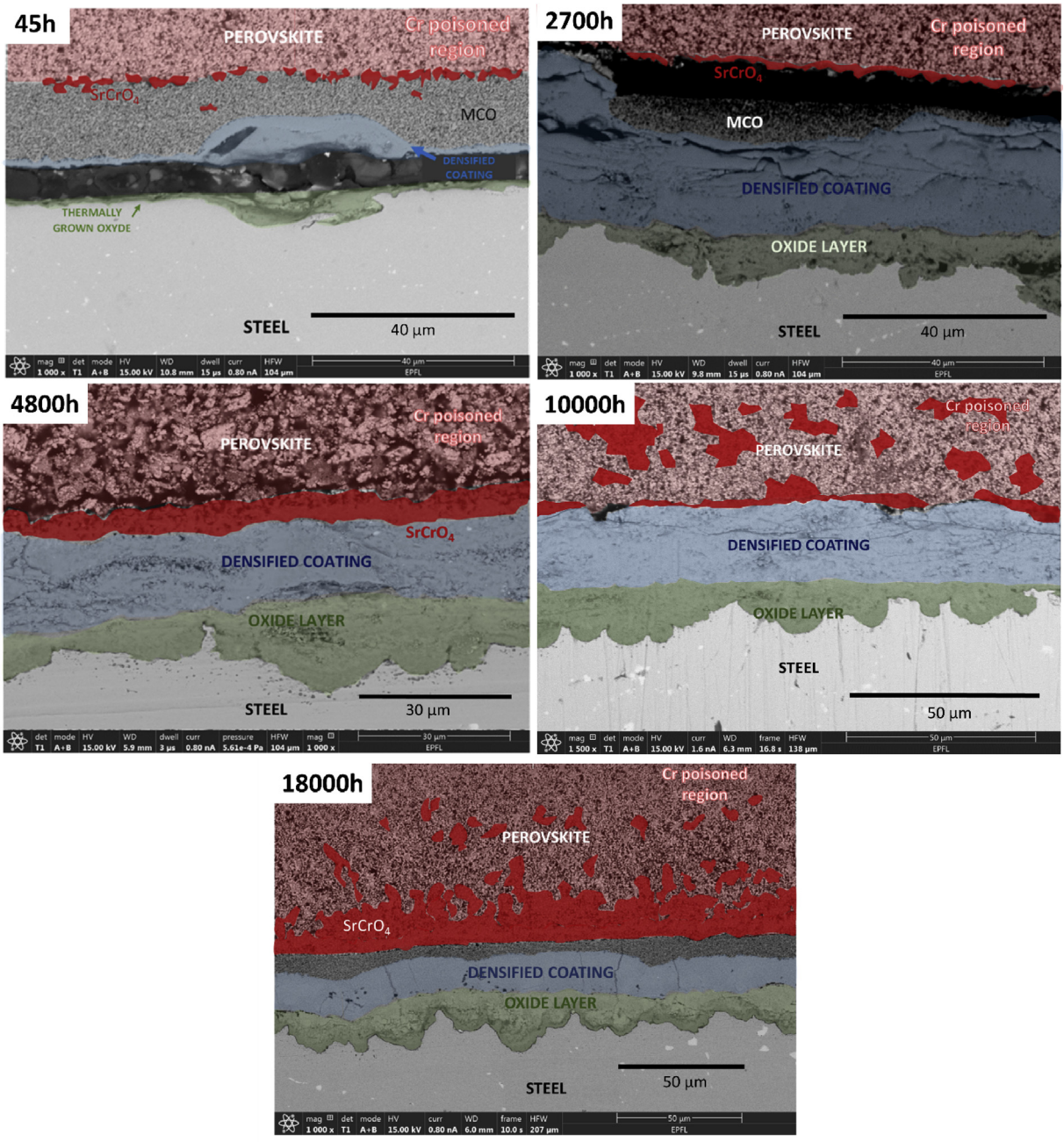

Fig. 2 – Time evolution of the interface at the cathode side rib. Light red coloured regions indicate the chromium-poisoned perovskite, dark red the presence of SrCrO4 reaction product, blue the densified MCO coating and green the oxide layer. (For interpretation of the references to color in this figure legend, the reader is referred to the Web version of this article.)

being a first layer of SiO_2 and TiO_2 precipitates followed by an uninterrupted $Cr_2O_3/(Cr,Mn)_3O_4$ layer. Bright Nb_2Fe Laves phases are visible in the steel substrate too. Nb-precursors of Laves phases are inserted in the steel on purpose, to improve the mechanical resistance of the steel to creep [21]. Between 10000 and 18000 h operation, the passivation layer failed, with Fe infiltrating the coating. The oxide layer is now irregular due to inward corrosion.

Thermal stress caused by the CTE difference between metallic and ceramic phases could potentially lead to adhesion failures, but at the metal/oxide interface the adhesion remains good. Fig. 4 presents a small crack in the 2700 h sample at the scale/MCO interface and a bigger delamination in the 45 h sample between the steel substrate and the scale. These defects are actually not representative of the global status of the MIC; moreover, they could also be induced by sample preparation. In the observation of large areas of the

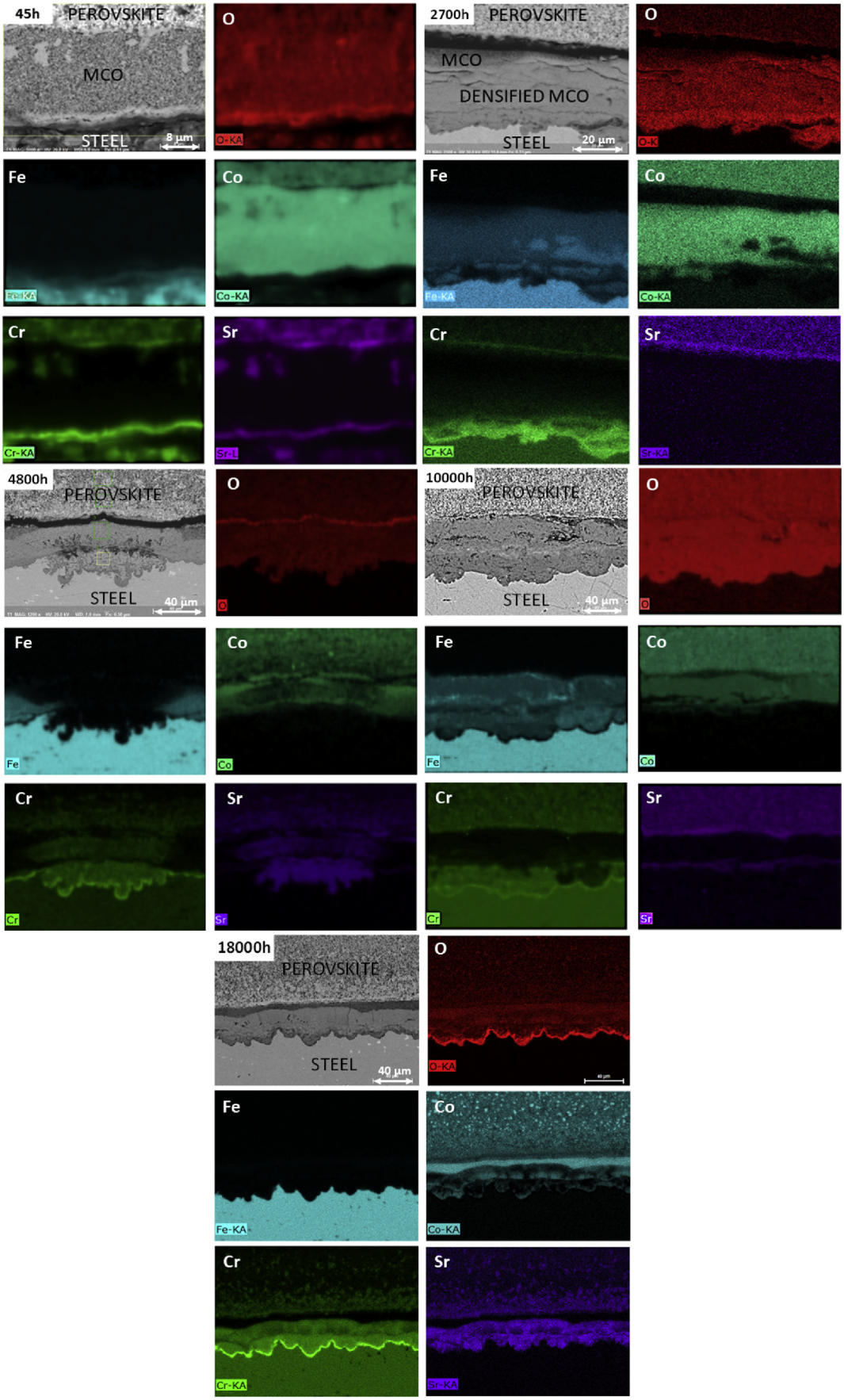
45h
PEROVSKITE
MCO
STEEL
8 µm
O
O-KA
2700h
PEROVSKITE
MCO
DENSIFIED MCO
STEEL
20 µm
O
O-K
Fe
Fe-KA
Co
Co-KA
Fe
Fe-KA
Co
Co-KA
Cr
Cr-KA
Sr
Sr-L
Cr
Cr-KA
Sr
Sr-KA
4800h
PEROVSKITE
STEEL
40 µm
O
O
10000h
PEROVSKITE
STEEL
40 µm
O
O
Fe
Fe
Co
Co
Fe
Fe
Co
Co
Cr
Cr
Sr
Sr
Cr
Cr
Sr
Sr
18000h
PEROVSKITE
STEEL
40 µm
O
O-KA
Fe
Fe-KA
Co
Co-KA
Cr
Cr-KA
Sr
Sr-KA

MIC surface in fact the most of the MIC cross section was free from delamination.

Regarding Cr contamination, only <1 at. % traces have been found in MCO up to 10000 h by EDS chemical analysis (not shown). In the 18000 h stack, chromium diffused into the coating together with iron. Iron was found to infiltrate the coating up to 30 at.% in some locations. Chromium instead remained below maximally 5 at. %.

Dual exposure region = anode side & cathode side

In this region of the interconnect, uncoated steel is exposed simultaneously to the oxidizing and reducing environments, and it is not in direct electrical contact with the cell. It can be thought of as a thin steel plate lapped on one side by air and on the other side by fuel. The behaviour of ferritic stainless steel under dual atmosphere operation has begun to be investigated carefully, both in *ex situ* [4] and *in situ* [22] conditions, as hydrogen is suspected to hamper the steel passivation process at the air side.

Fig. 5 and Fig. 6 describe the scale evolution at both sides of the dual exposure plate. The scale composition is the same for both sides: a thin SiO_2 and TiO_2 layer just above the steel substrate, followed by Cr_2O_3, and $(Mn,Cr)_3O_4$. Other elements, notably Fe, are found only as traces. In Figs. 5 and 6, the white spots close to the steel/scale interface are Laves phases. In stacks #4800, #10000 and #18000, small and round TiN precipitates are observed too.

No spallation occurred in these two regions for any of the samples observed.

124 thermal cycles stack

Fig. 7illustrates the interfaces at the cathode side rib and cathode side valley, for stack #124 TC which underwent 124 thermal cycles (25°C–750 °C) within 2600 h of operation.

SEM observations at different magnification did not highlight any failure between the metallic and ceramic layers. This is important because for the valley region there is no stack compressive force acting that could prevent material spallation.

The only region showing local cracks is the interface between the scale and the densified coating at the cathode side rib (red dotted rectangles). The same type of cracks was also observed in stacks #2700, #4800, #10000 and #18000, again at the scale/densified coating interface. The absence of material spallation is confirmed also by the consistency in scale thickness with the other analysed stacks.

Cross sections of the dual exposure regions did not present delamination nor cracks, like in Figs. 5 and 6). Stack disassembling and sample preparation caused some defects.

Summary

Merging the information of the six stacks described and analysed above, the following main observations apply: 1) Diffusion of Fe into the MCO coating and its subsequent densification concerns principally the cathode side rib region, where the MIC is in direct contact with perovskite. The cathode side valley of stack #18000 being the only exception; 2) Sr from the perovskite migrates towards the MIC and interacts with Cr contained in the steel to form $SrCrO_4$; 3) $SrCrO_4$ can form both at the coating/perovskite interface or on the steel surface; 4) regarding dual atmosphere exposure and corrosion, the scale compositions present no Fe contamination or hematite-like zones; 5) good adhesion of the ceramic layers to the steel substrate and absence of spallation is observed, but porosity at the interface between the scale and the densified coating may be present.

Discussion

Passivation layer failure

Not shown in Fig. 3, silicon oxide presents a double occurrence in the regions affected by Fe breakaway: one line at the scale/coating layer interface and a second and thinner layer moving together with the Cr_2O_3/steel interface. The SiO_2 profile follows the inward evolution of the steel/oxide interface confirming that there has been a corrosion inside the steel substrate. Also in stack #18000, Si presents a discontinuous distribution at the cathode side rib. This indicates that at least up to 18000 h, silica does not give rise to electrical insulation. The fragmented distribution of the SiO_2 layer is a positive side effect of the inward corrosion.

Iron infiltration in the MCO coating is observed in all the samples. Literature describes the reaction between Cr_2O_3 and MCO as an opposite interdiffusion of Cr-ions towards the spinel coating and Mn- and Co-ions towards the chromia scale [18]. Two different reaction layers should hence be formed: $(MnCo)Cr_2O_4$ close to Cr_2O_3 and $(MnCoCr)_3O_4$ close to the MCO protective layer [23].

This phenomenon has been commonly observed, while Fe-cation infiltration into MCO is not reported in any of the cited studies. The undesirable appearance of iron oxides on the stainless steel surface due to the failure of the passivation layer is known as iron breakaway. On the other hand, iron contamination of MCO spinel as such is not harmful, in fact improving its electrical conductivity [24]. Problems might arise if Fe segregates as oxide alone [25].

Iron breakaway originates from two possible causes: intrinsic chemical failure (InCF) or mechanically induced chemical failure [26]. In the first case, the Cr-ions supply from the alloy substrate is not fast enough to sustain the oxidation process. In practice, this translates into a minimum Cr concentration value (N_{Cr}^{min}) at the metal/oxide interface to guarantee passivation. In order to assess if the InCF process occurred in the investigated stacks, N_{Cr}^{min} was calculated using the approach given by Othman and co-workers [27], in turn derived from Wagner's theory [28].

For the calculation, two different diffusion coefficient values are taken into consideration: a conservative $2 \cdot 10^{-12}$ $cm^2 s^{-1}$ [27] and a more optimistic $7.4 \cdot 10^{-13}$ $cm^2 s^{-1}$ [29]. The

Fig. 3 – EDS elemental map of regions similar to those of Fig. 2. The presence of the Sr Kα emission peak (14.14 keV) confirmed that strontium is not an artefact due to the Si X-ray Ka emission peak (1.74 keV).

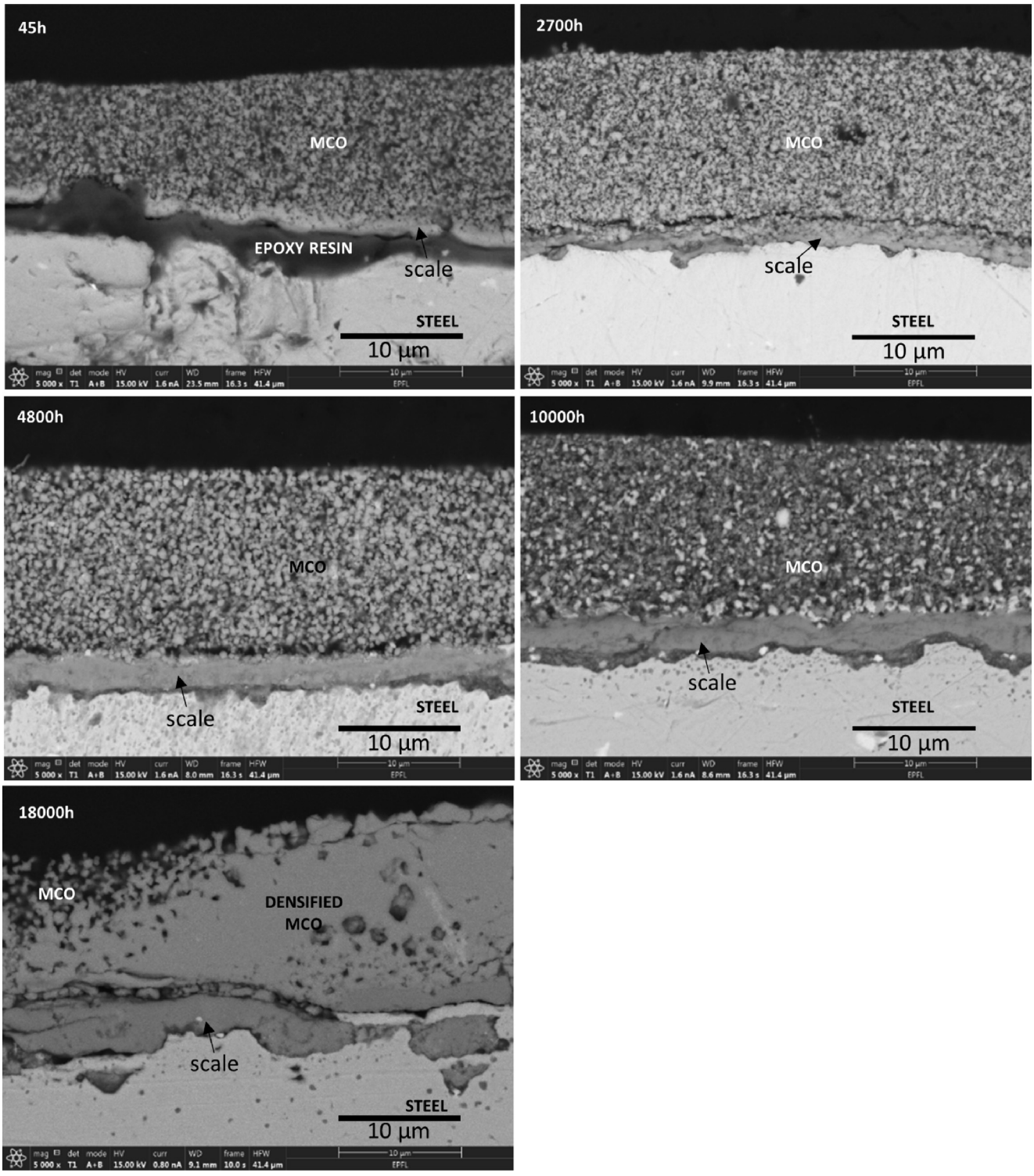

Fig. 4 – Time evolution of the steel/MCO interface at the cathode side valley.

rate constant (K_p) is taken from [23] after being converted from $g^2cm^4s^{-1}$ to cm^2s^{-1}.

The result gives N_{Cr}^{min} = 8.9 wt% and 12.4 wt% for the 2 scenarios. These values are compared with the depletion profiles for stacks #45 and #2700 (Fig. 8) at the cathode side rib and valley positions. Red lines represent the Cr content profile and lilac lines represent the Fe content profile, while the black dotted vertical line indicates the steel/scale interface.

In stack #45 the Cr depletion region starts 10–15 µm below the steel/oxide interface with a marked decrease in the 8–10 µm closest to the interface. The chromium content in the steel just below the scale is around 10 wt% at the cathode side

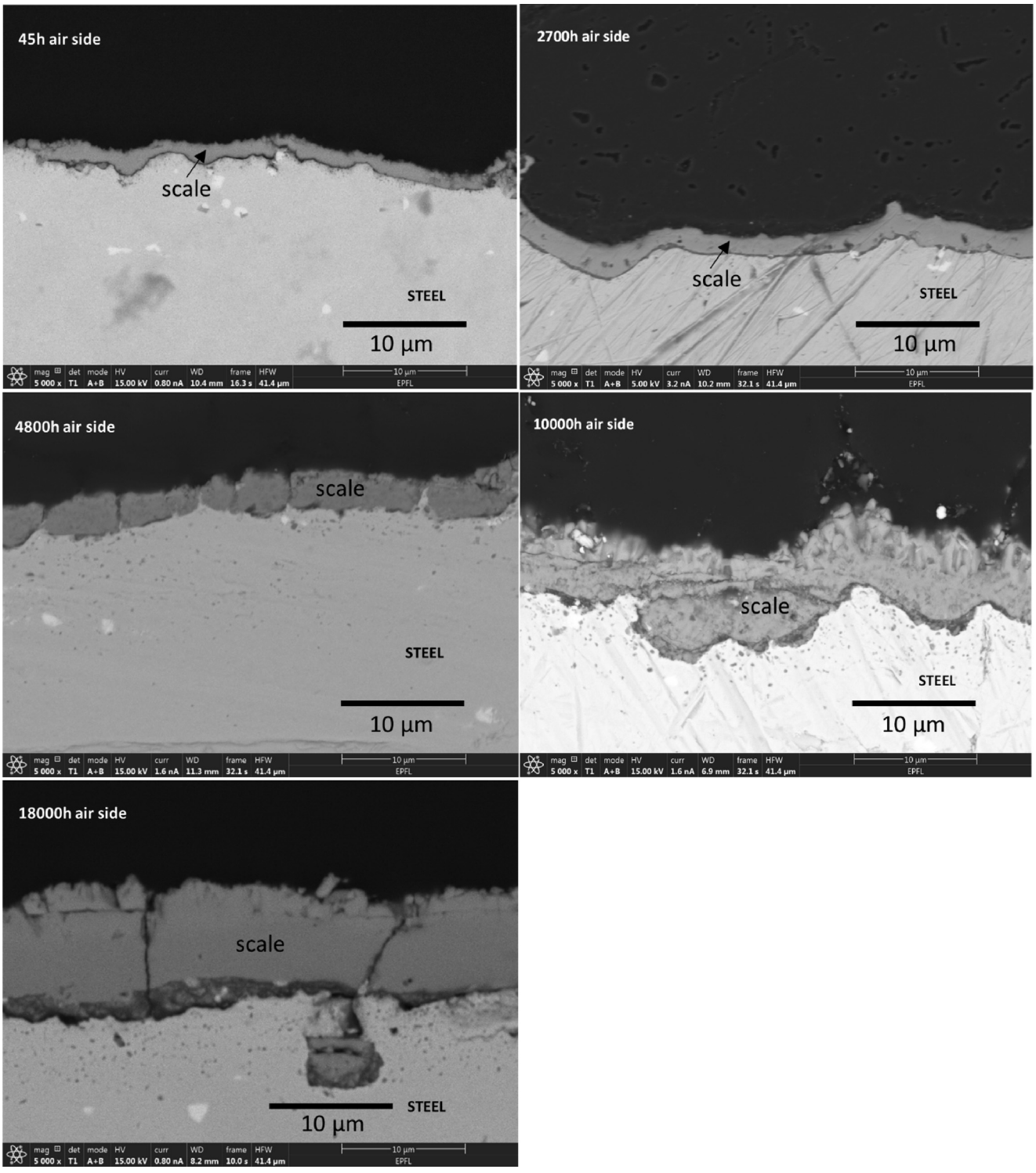

Fig. 5 – Time evolution of uncoated steel surface at the air side (cathode) of a dual exposure region.

valley and less than 8 wt% at the cathode side rib coherent with inward corrosion (matching with Fe breakaway cf. Fig. 2 and 45 h). Additional chromium quantification in the steel beneath the inward corrosion region at the cathode side rib of stack #45 recorded ca. 6 wt% of Cr.

In stack #2700 instead, the corrosion kinetics slowed down, with a re-homogenization of the Cr content in the steel below the scale of ca. 15 wt% in both the valley and the rib region.

Even considering the limitation of the Wagner theory, the comparison of measured values at the cathode side rib with

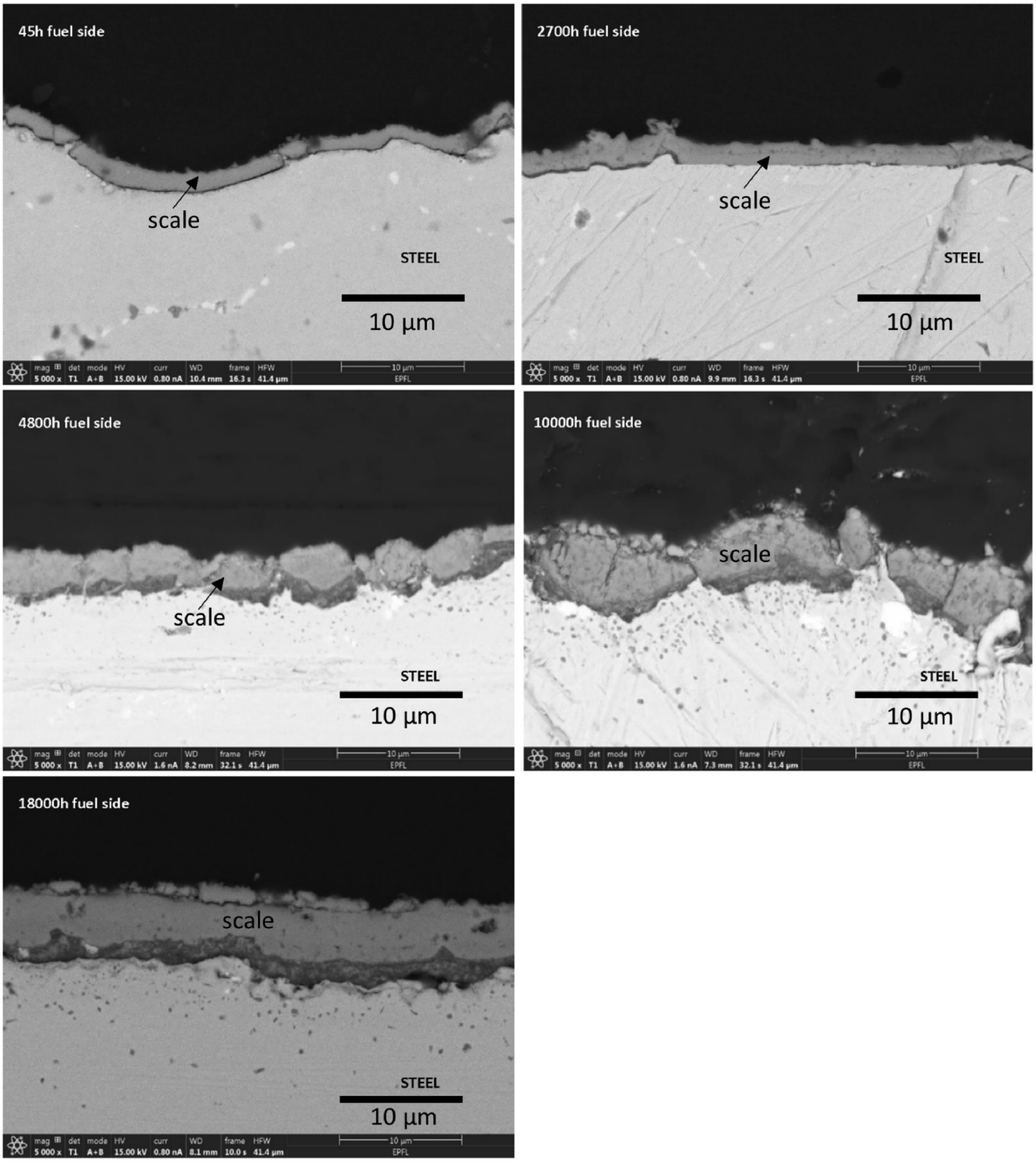

Fig. 6 – Time evolution of uncoated steel surface at the fuel side (anode) of a dual exposure region.

the calculated N_{Cr}^{min} values indicate that InCF could be a cause for passivation layer failure. The chromium profiles also indicate that the corrosion process tends to slow down and the Cr distribution in the steel to homogenize in the first months of operation.

The difference in Cr wt.% between the standard and inward corrosion in stack #45 suggests the presence of an element or substance removing chromium. In ferritic stainless steel degradation studies, this could typically be steam, but the absence of Fe breakaway at the cathode side valley below 10000 h of operation indicates that steam alone cannot explain all observations.

Alternatively, strontium could be the chromium binding element. Gibbs free energy equilibrium values indicate $SrCrO_4$ to be a favoured species over Cr_2O_3 in the 700–800 °C temperature range [30]. Strontium chromate formation in SOFC

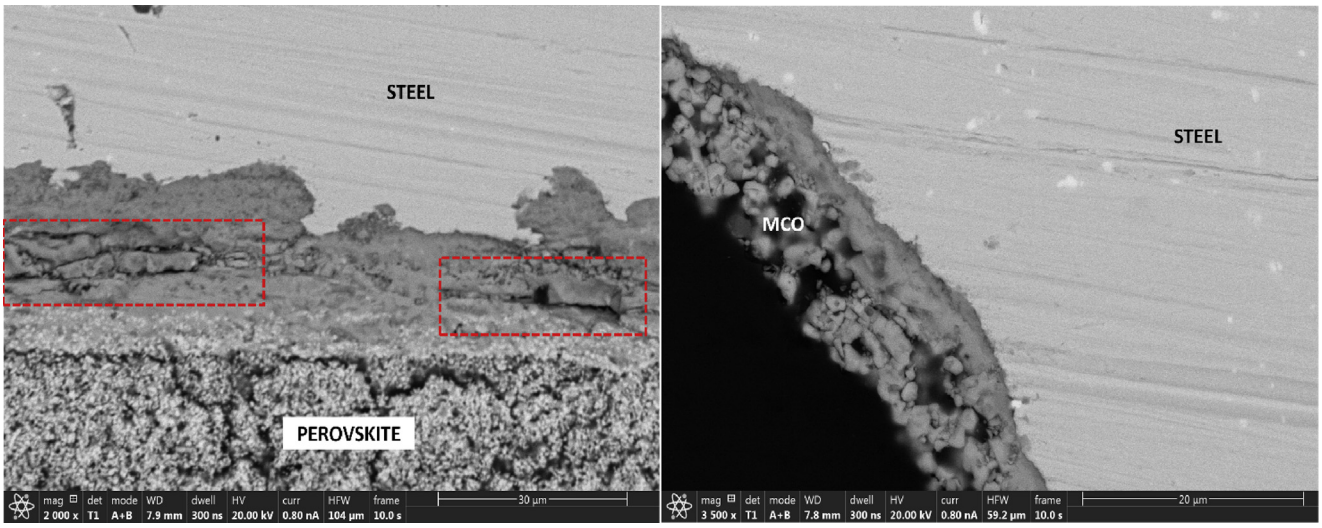

Fig. 7 – Micrograph of the cathode side rib (left) and cathode side valley (right) regions of interest taken from a stack which underwent 124 thermal cycles.

operating conditions is harmful for the cell lifetime, as it is a poorly conductive phase (ρ_{SrCrO4} = ~10^3 Ωcm^{-1}) [31] and decreases the oxygen surface exchange reaction sites [32]. Besides electrode poisoning, strontium chromate passivation on the steel surface is undesirable too due to the risk of electrical insulation.

As shown in Fig. 2, already in the first hours of stack operation, the perovskite is not stable and Sr moves towards the steel. EDS chemical analysis indicated the dense aggregates at the MCO/perovskite interface to be compositionally close to $SrCrO_4$ and found Sr and Cr inside the MCO coating too: traces of strontium close to the thermally grown scale were found already in stack #45.

Segregation of strontium oxide on perovskite surfaces is a known degradation issue [33]. Strontium cations could have migrated from the perovskite through a solid or a gas diffusion mechanism. A study describing experimental conditions similar to ours proposed a solid diffusion mechanism for strontium contamination [34]. However, in different MICs containing dense barrier layers and tested in the same conditions reported here, no strontium diffusion through the coating was observed. For example, this is the case when MCO

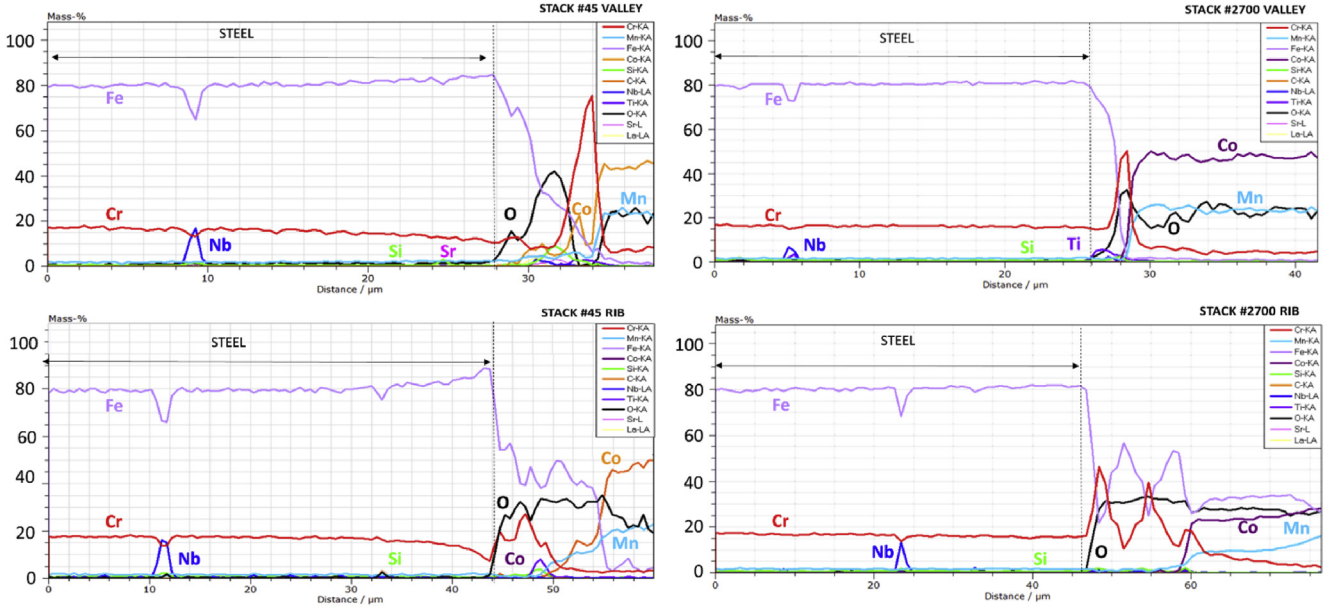

Fig. 8 – Elemental profile (wt. %) of cathode side valley and rib in stack #45 and #2700. The scanning starts in the bulk on the alloy substrate and ends in the thermally grown oxide layer. Note the Cr profile in proximity of the steel/scale interface.

was deposited via physical vapour deposition. In SRUs coated via PVD, strontium cations accumulated at the perovskite/MCO interface, not passing this border. The absence of strontium diffusion via the solid phase has been recently confirmed by another stack analysis [9].

At the same time, Sr vapours are thermodynamically possible in our testing conditions. It can therefore be suggested that strontium moved through the gas phase and that steam in the air flow triggered Sr evaporation. Most of the vapour is carried away by the air flow and therefore not affecting the cathode side valley regions.

Regarding mechanically induced iron breakaway corrosion, it refers to random passivation failure due to machining. Some regions with enhanced corrosion could match this explanation, but final proof is lacking.

Chromium contamination too is suspected to occur via the gas phase. The chromium distribution profile between the scale and the perovskite does not follow a typical diffusion trend and the amount of Cr inside the fully densified MCO in stack #10000 was ca 1 at%. This suggests that Cr migration stopped after full densification of the MCO in contact with the perovskite. Analysis on PVD-coated MICs confirmed the absence of chromium contamination of the perovskite in the case of dense coatings [35].

The distribution profile of iron and its ionic compatibility with Mn and Co suggest instead a solid phase diffusion process.

The latest considerations indicate that a dense coating would be technologically preferable over a porous one, because it would hinder the diffusion of the gas phases and subsequently the interaction between interconnect and cathode. On the other hand, SOFC commercialization is related to decreasing stack manufacturing cost. In this sense, wet powder sprayed coatings are more readily used than, for example, physical vapour deposition or atmospheric plasma spray. The latter coating techniques require longer deposition time or use more material, respectively. One of the aims of this study is to evaluate if commercially oriented solutions can be reliable for long term use in industrial SOFC stacks. The observed stabilization of degradation processes after 5000 h tends to confirm this, and therefore even a porous coating can be a reliable compromise in terms of quality/cost.

The literature on Fe-breakaway is rather scarce. Few papers described the MIC behaviour in stacks over long operating periods; less still are those operated at similar conditions to the stacks analysed in this work. Haanappel et al. [25] found iron oxide formation on top of the MICs, but the reacting element in this case was Pb contained in the sealing material. As another example, a 3-cell stack containing AISI 441 MICs coated with Ce-(Mn,Co) was run for 6000 h, but no specific lifetime issues were found, notably no sign of Fe-breakaway even at the MIC/perovskite interface (LSM) [10]. Recently, uncoated SUS430 MICs have been employed in a 5-cell short stack [22]. Even if the test period was short, Fe-breakaway occurred with Fe_2O_3 found at the steel/cathode interface.

In the MICs analysed in the present work instead, Fe substituted for Mn and Co, preventing the formation of pure iron oxide. Accumulation of Mn at the border of the growing densified coating suggests a preference for Mn-substitution. The fact that stacks #4800 and #10000 show similar average concentration values may indicate a stabilization of the corrosion process. Regarding the long time reliability of stack operation, thermodynamic stability of Fe-infiltrated MCO should not be a problem as it is more stable than Mn_3O_4, Fe_3O_4 and Co_3O_4 alone [36].

Oxide growth

Fig. 9 shows the scale thickness growth curves obtained by measuring the average scale thicknesses of the different regions of interest of the interconnects. The values of these curves consider the whole scale and not chromia alone; most of the literature curves refer to pure Cr_2O_3 growth only. Values from stack #2700 are reported separately because this stack was operated at a lower average temperature than the others. This does not change the corrosion product composition, but slows down the kinetic growth, as corroborated from the data in Fig. 9.

High temperature corrosion processes are usually described with the model proposed by Wagner [28]. The oxide formation process is driven by diffusion of cations and anions through the growing dense scale, and the relation scale thickness/time on a plot would then assume a parabolic trend – the same as for Fick's law. Nevertheless, the theory is basic [37], leaving aside chemical interactions or the presence of alternative diffusion paths to lattice diffusion only. The curves extrapolated in Fig. 9 in fact do not follow the parabolic trend.

The "cathode side rib" curve shows a capacitance-like trend, with a sharp decrease in the growth rate after 5000 h, and the corrosion process being enhanced mostly during the first few thousand hours of operation. (cf. Figure 2, 45 h and 2700 h). It is interesting to note that the thickness value of the scale at the cathode side rib for the stack #2700, despite its lower average operating temperature, would nonetheless match the general trend, indicating that the materials chemical interaction may dominate the first stage of the corrosion process in this region of interest.

Applying a trend line to the empirical curve of Fig. 9, a forecast to longer operation time would give at 40000 h an average scale thickness of 13.3 μm and at 80000 h of 14.4 μm, not adding substantially to long term resistive loss compared to the situation after 5000–10000 h.

The "cathode side valley" curve shows a different trend line than that of the "cathode side rib". This difference too confirms the influence of the perovskite on the MIC degradation process.

The corrosion behaviour of this interface can be divided in two regions. Up to 10 000 h, a parabolic trend line with $K_p = 3*10^{-19}$ cm^2sec^{-1} would fit the few data points. A validation of this value with data from literature is difficult, as the combination of materials and the operating conditions involved is difficult to find. Two compatible studies provide values of growth rate orders of magnitude bigger, $4*10^{-16}$ cm^2sec^{-1} [38] and $6*10^{-15}$ cm^2sec^{-1} [39] respectively. The reasons for this difference are the higher temperature of their tests (800 °C), the curve in Fig. 9 does not follow exactly a parabolic trend and the longer period of oxidation of the MIC (the samples of the cited studied have been tested < 1000 h). In any case, the comparison is interesting because the growth rate at the cathode side is slower than expected from laboratory conditions.

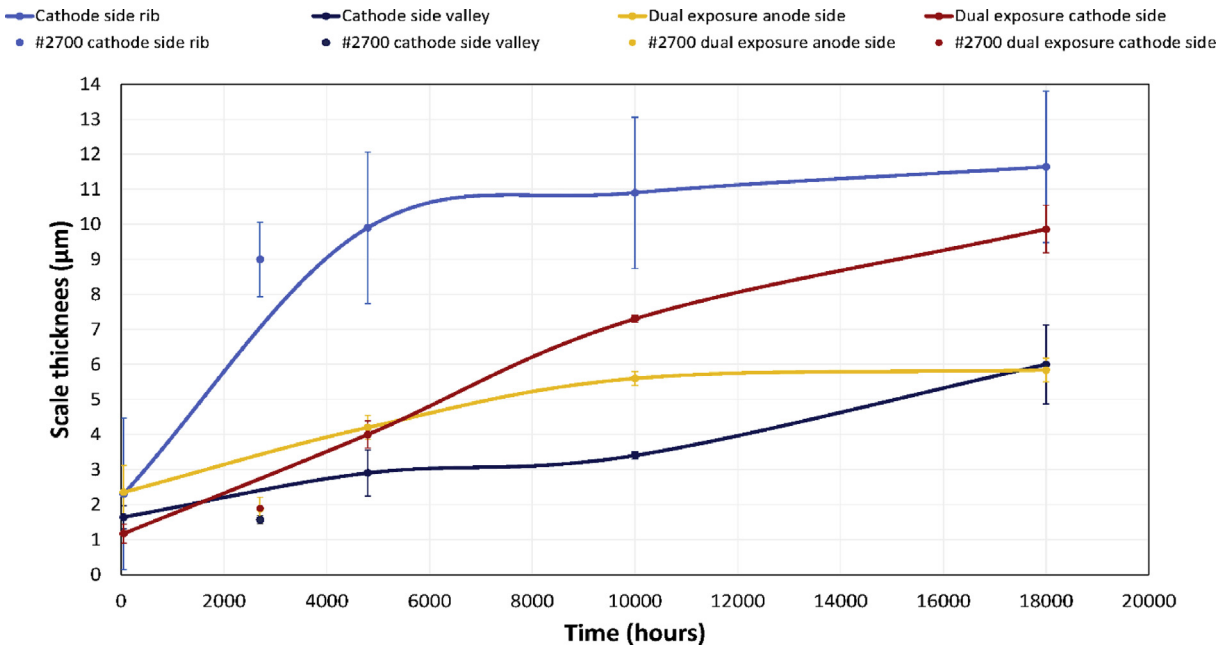

Fig. 9 – Scale evolution with time at different MIC interfaces. Points of stack #2700 are reported but not included in the forecasting models.

The elemental scale composition, however, is coherent with expectation: SiO_2 precipitates followed by Cr_2O_3 and $(CrMn)_3O_4$ layers. After 10000 h, iron breakaway occurs, as indicated by the curve rising again. A quantitative forecasting of the final scale thickness at the cathode valley side is not possible, even though a stabilization – similar to what happened at the cathode side rib-after the complete coating densification is likely to be expected.

The "dual exposure plate (anode and cathode side)" experienced simultaneous exposure to oxidizing and reducing atmospheres. This condition is potentially harmful for the steel as an iron oxide phase could form on top of the Cr_2O_3 oxide at the cathode side [22]. EDS analysis at the cathode side of the dual plate instead revealed Cr_2O_3+$(CrMn)_3O_4$ oxides. In a recent paper, the appearance of iron oxides on top of the scale of uncoated AISI 441 exposed to H_2/air dual atmosphere was associated to temperature, i.e. this phenomenon occurs at aging temperatures lower than 700 °C [4]. This explanation does not match with a different study of AISI441 oxidation behaviour, under similar dual atmosphere at 800 °C, where iron oxide is found top of the scale [40]. Since the AISI441 samples of the former study underwent a pre-oxidation process while that of the second study did not, the pre-operational aging that the MICs underwent due to coating sintering has positively influenced the corrosion behaviour of the steel [41]. The deviation of the growth curve from the parabolic trend could instead be explained by hydrogen diffusion from the fuel side towards the air side. Hydrogen ions dissolved in the steel substrate would enhance metal vacancy formation in chromia and this in turn lead to faster transport of Cr-cations [42]. On the other hand, MIC pre-oxidation is likely to mitigate this phenomenon too [40].

Oxide growth at the "dual exposure anode side" follows a trend with slower kinetics than that obtained via experiments performed in laboratory conditions. The curve drawn through the average values becomes a perfect plateau after 10000 h, indicating a complete stabilization of the corrosion process. Realistically, the scale will still grow at a low rate; considering the curve passing through the maximum of each point the forecasted values will be 6.4 µm and 6.9 µm at 40000 and 80000 h.

From the observations on the four regions of interest, the steel oxide growth is not expected to cause stack failure. Formation of a continuous SiO_2 layer below the scale is the main concern in terms of maintained conductivity of the MIC. Niobium addition and limited content of Si in the alloy composition should hinder the creation of such insulating layers. The literature in this sense does not provide answers for long term extrapolation, suggesting to look instead for *in situ* long term testing [43]. From the observations on the stacks in our study, Si oxidation appears to be stabilizing between 4800 h and 10000 h. Observations on stack #18000 confirmed that no further changes in silica layer morphology or thickness were apparent.

With the scale composition not exactly measurable, it is not possible to precisely quantify the contribution of the interconnect scale to the stack degradation process in terms of ohmic losses.

From the observations presented, however, this contribution will tend to stabilize after 5000 h and therefore not present a main problem for long-term degradation. To counterbalance the initial increase of the scale ohmic resistance, the coating densification due to Fe-incursion in fact improves the conductivity of the spinel. Formation of $SrCrO_4$ inside the perovskite cathode is also related to the initial stage

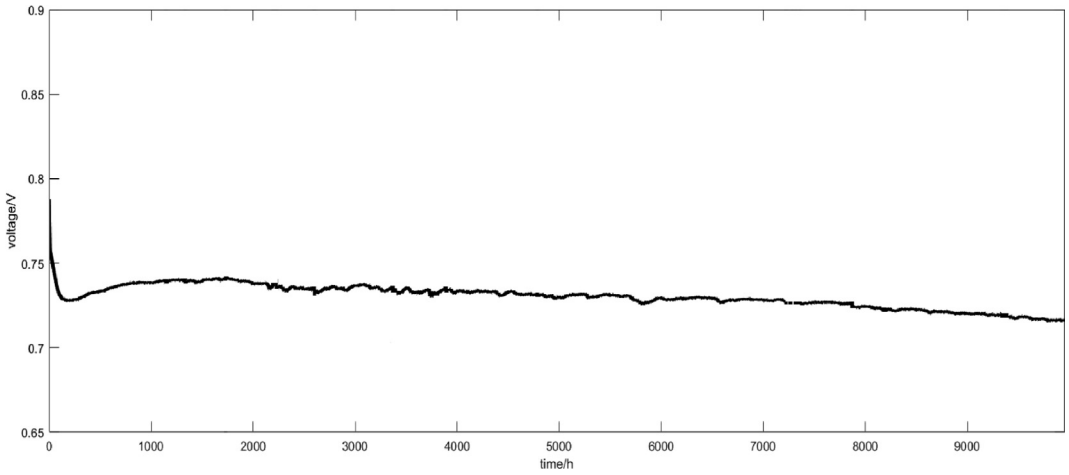

Fig. 10 – Average voltage evolution over time of a single repeating unit from a MIC coated with porous MCO in a stack tested for 10000 h.

of operation as, after coating densification due to Fe-breakaway, the Cr-migration will decrease. Looking at Fig. 10, the degradation in a SRU containing a MIC coated with a porous MCO is mild (<1%/kh). This value is obtained on average between two identical SRUs tested in the stack #10000. In the initial period of 2500 h the voltage value is not stable. Considering that the corrosion process at the MIC/perovskite interface occurs mostly during the first 5000 h of operation, a correlation between the two phenomena is likely. On the other hand, it is not possible to distinguish between the cumulated cell and MIC ohmic loss contributions.

Fig. 10 also confirms a stabilization in the degradation process after 5000 h, with the curve being linear in the 2500–10000 h range.

Merging the information from Figs. 2, Figs. 9 and 10, the type of interconnect studied in this article should not limit the stack lifetime. According to observations in stack #124, also a sudden shut down of the stacks should not lead to contact issue from the MIC side.

The main risk for stack lifetime limitation originating at the cathode side therefore would be the complete covering of $SrCrO_4$ on the steel underneath the protective coating.

Mechanical Properties

The interface between the oxide and the steel substrate survived the stresses induced by the thermal cycling treatment. The coefficient of thermal expansion (CTE) for K41/AISI441 is $12.8*10^{-6}$ K^{-1} in the 20–800 °C range [16] while for Cr_2O_3 it is $5.7*10^{-6}$ K^{-1} in the 20–1000 °C range [44]. In the presence of native scale prior to heating, as for the MICs studied in this manuscript, this difference induces tensile stresses in the scale during heat up and compressive stresses during cooling. Hence, the repetition of thermal ramps could induce delamination between the oxide and the metal phases, eventually decreasing the contact surface between the MIC and the cell and triggering accelerated corrosion of the metal surface. In addition, another element of risk lies in the difference in CTE among ceramic phases too, i.e. the multiple oxide layers created.

From the stacks observed, however, the difference in CTE values between metallic and ceramic phases did not lead to delamination. The densification of the MCO coating, instead, caused cracks, but in none of the observed cross sections these cracks lead to destructive failure. Similarly, small fractures at the scale/densified layer interface were commonly found. Again, none of these caused mechanical issues. Compression of the stack is thought to have a beneficial influence.

Comparing these results with literature, few authors focused their attention on mechanical aspects of the MIC compared to that of the ceramic cell, but in all cases the energetic approach was used. A certain stress threshold must be reached for the cracks to propagate and the adhesion between layers to fail. In the specific case of metal interconnects, the two interesting interfaces are the steel/scale and scale/protective coating. The parameter taken into account to determine whether the contact will resist is the scale thickness: Liu et al. for example measured the maximum shear stress tolerated by the steel/scale and scale/coating for MCO-coated Crofer 22 APU with a Rockwell indentation test [45]. According to their model, the predicted lifetime was 4800 h for uncoated Crofer 22 APU (critical scale thickness 11.4 μm) and 15000 h for coated Crofer 22 APU (critical scale thickness 4.2 μm). Interestingly, the lifetime limit for the uncoated ferritic stainless steel matches the operating time of one of the stacks. However, stack #4800 showed no spallation of the oxide layer in the dual exposure (uncoated) region. It follows that the MIC is more reliable than what was predicted by this model, moreover accounting for the fact that K41 is a supposedly inferior steel to Crofer 22 APU. For the coated case, the comparison of the results is difficult as the scale grown on the MIC in the stack is not Cr_2O_3 only; nonetheless, 11 μm of scale thickness were reached after 10000 h of operation, yet no serious failure of the interface was found in this case either.

Underestimation of the beneficial effect of compression against spallation could be a reason for the mismatch between this model and operation reality. The observation on a stack run for 35000 h at FZJ demonstrated the reliability of ferritic stainless steel for this long term operation [46].

Conclusions

This article presents an encompassing description of long-term degradation phenomena taking place for commercial solid oxide fuel cell (SOFC) interconnects tested in real stack conditions. Five short stacks, containing identical parts, have been tested for 45, 2700, 4800, 10000 and 18000 h under air and H_2/N_2 and subsequently cross sectioned and observed by scanning electron microscope (SEM) coupled with energy dispersive X-ray spectroscopy (EDS). New and important insights regarding the reliability of the low cost K41/AISI441 steel grade as metal interconnect are presented. The current few studies in literature on stack degradation evolution focus on the more expensive steel grade Crofer 22 APU or H. This work, in demonstrating the long-term reliability of AISI441/K41 interconnect, points to stack cost reduction using wider available commercial steel grades.

In addition, a stack that underwent 124 thermal cycles was post-test analysed as well to focus on the mechanical behaviour.

The following conclusions are drawn:

- The electrical contact region between the MIC and the cathode perovskite is chemically the most active. Strontium migrates from the first operating hours towards the steel. It reacts with chromium, affecting the Cr_2O_3 passivation layer. This can lead to chemical failure-induced Fe-breakaway corrosion or formation of $SrCrO_4$ on the steel surface.
- Iron breakaway triggers densification of MnCo-spinel which becomes infiltrated with Fe (>30 at.%). This reaction, however, should not harm stack lifetime as (Cr,Fe,Mn) spinels are thermodynamically stable and will not separate into fragile and low conductive hematite phases.
- Spinel densification appears to have positive effects on the Cr barrier property of the coating on the long term.
- The main stack degradation risk is the formation of $SrCrO_4$ on top of the stainless steel substrates, increasing ohmic losses. This phenomenon is in competition with Fe-breakaway and was found in stacks #4800, #10000 and #18000.
- A discontinuous SiO_2 layer forms in the electrical contact regions up to 18000 h. From the observations it is not expected for even longer operating time that silica should cause electrical insulation.
- The empirical model obtained from micrograph thickness measurements predicts a stabilization in corrosion after ca. 5000 h of operation for all the regions of interest but the uncoated steel at the cathode side of the dual atmosphere exposed plate region. According to the curves, average scale thicknesses at the cathode side ribs will be $\approx$ 13.3 μm and $\approx$14.4 μm respectively at 40000 h and 80000 h. The contribution of the MIC component to the ohmic losses at the steel/cell interface tends to stabilize. The presented data can be more valuable for oxide growth modelling, as most data for modelling work are typically based on *ex-situ* tested samples.
- At the cathode side valley, the passivation layer fails between 10000 and 18000 h. This supports that Fe breakaway corrosion in AISI441 is caused by intrinsic chemical failure process and that strontium is a catalyser of this process.
- In the uncoated interconnect region (Figs. 5 and 6), a scale made of discontinuous SiO_2, dense Cr_2O_3 and $(Mn,Cr)_3O_4$ spinel on top is found on both anode and cathode exposed sides. No traces of hematite phases were seen at the cathode air side on any sample, contrarily to what was reported before from specific dual atmosphere tests on ferritic stainless steel. This may be due to preoxidation of the MIC. This confirms that AISI441/K41 is suitable for working in IT-SOFC conditions.
- No material spallation was found in the four regions analysed. Overall, the adhesion between the different phases was good and any detachment found during observations was likely caused by the disassembling and polishing processes. The porosity found at the scale/densified coating interface is not considered to be harmful, as stack compression demonstrated to avoid delamination.
- The absence of spallation of the oxide layer from the steel substrate can be confirmed from a stack that underwent 124 thermal cycles (Fig. 7). The SEM/EDS post operando images found some cracks only in the region between the oxide layer and the ceramic coating. Even though, this did not lead to the loss of the coating.
- In general, *ex-situ* tests on MIC materials demonstrated not always to be representative of the real degradation behaviour of the ferritic stainless steel in a stack. Degradation in a stack was less negative than predicted from models found in literature for both the corrosion and mechanical resistance behaviours.

Acknowledgement

This work has been conducted within the SCoReD2.0 and SOSLeM projects, which have received funding from the European Union's Fuel Cells and Hydrogen Joint Technology Initiative under contract no. 325331 and 700667 respectively. For Swiss partners SOSLeM was funded by the Swiss State Secretariat for Education Research and Innovation (SEFRI) under contract 16.0042. The FCH-JU-funded ENDURANCE project (grant agreement no. 621207) supplied important samples for the study. The authors want also to thank SOLIDpower s.p.a. and HTceramix for the kind collaboration in the analysis process.

REFERENCES

[1] Bertoldi M, Bucheli O, Ravagni A. Development, manufacturing and deployment of SOFC-based products at SOLIDpower. ECS Trans 2017;78:117–23.
[2] Zhu WZ, Deevi SC. Development of interconnect materials for solid oxide fuel cells. Mater Sci Eng A 2003;348:227–43. https://doi.org/10.1016/S0921-5093(02)00736-0.
[3] Wu J, Liu X. Recent development of SOFC metallic interconnect. J Mater Sci Technol 2010;26:293–305. https://doi.org/10.1016/S1005-0302(10)60049-7.
[4] Alnegren P, Sattari M, Svensson J-E, Froitzheim J. Temperature dependence of corrosion of ferritic stainless

steel in dual atmosphere at 600–800 °C. J Power Sources 2018;392:129–38. https://doi.org/10.1016/j.jpowsour.2018.04.088.
[5] Frangini S, Masi A, Seta LD, Bianco M, Herle JV. Composite Cu-LaFeO3 conversion coatings on a 18Cr ferritic stainless steel for IT-SOFC interconnects: effect of long-term air exposure at 700°C on Cr diffusion barrier and electrical properties. J Electrochem Soc 2018;165:F97–104. https://doi.org/10.1149/2.0101803jes.
[6] Ardigo-Besnard MR, Popa I, Chevalier S. Effect of spinel and perovskite coatings on the long term oxidation of a ferritic stainless steel in H2/H2O atmosphere. Corros Sci 2019;148:251–63. https://doi.org/10.1016/j.corsci.2018.12.034.
[7] Young DJ, Zurek J, Singheiser L, Quadakkers WJ. Temperature dependence of oxide scale formation on high-Cr ferritic steels in Ar–H2–H2O. Corros Sci 2011;53:2131–41. https://doi.org/10.1016/j.corsci.2011.02.031.
[8] Scataglini R, Wei M, Mayyas A, Chan SH, Lipman T, Santarelli M. A direct manufacturing cost model for solid-oxide fuel cell stacks. Fuel Cells 2017;17:825–42. https://doi.org/10.1002/fuce.201700012.
[9] Menzler NH, Sebold D, Guillon O. Post-test characterization of a solid oxide fuel cell stack operated for more than 30,000 hours: the cell. J Power Sources 2018;374:69–76. https://doi.org/10.1016/j.jpowsour.2017.11.025.
[10] Chou Y-S, Stevenson JW, Choi J-P. Long-term evaluation of solid oxide fuel cell candidate materials in a 3-cell generic stack test fixture, part III: stability and microstructure of Ce-(Mn,Co)-spinel coating, AISI441 interconnect, alumina coating, cathode and anode. J Power Sources 2014;257:444–53. https://doi.org/10.1016/j.jpowsour.2013.11.086.
[11] Fleischhauer F, Tiefenauer A, Graule T, Danzer R, Mai A, Kuebler J. Failure analysis of electrolyte-supported solid oxide fuel cells. J Power Sources 2014;258:382–90. https://doi.org/10.1016/j.jpowsour.2014.02.009.
[12] Yan D, Liang L, Yang J, Zhang T, Pu J, Chi B, et al. Performance degradation and analysis of 10-cell anode-supported SOFC stack with external manifold structure. Energy 2017;125:663–70. https://doi.org/10.1016/j.energy.2016.12.107.
[13] Yang J, Yan D, Huang W, Li J, Pu J, Chi B, et al. Improvement on durability and thermal cycle performance for solid oxide fuel cell stack with external manifold structure. Energy 2018;149:903–13. https://doi.org/10.1016/j.energy.2018.02.072.
[14] Budiman RA, Bagarinao KD, Liu SS, Cho DH, Ishiyama T, Kishimoto H, et al. Time-Dependence of surface composition, transport properties degradation, and thermodynamic consideration of La0.6Sr0.4Co0.2Fe0.8O3-δ under chromium poisoning. J Electrochem Soc 2018;165:F1206–16. https://doi.org/10.1149/2.0721814jes.
[15] Jiang SP. Development of lanthanum strontium cobalt ferrite perovskite electrodes of solid oxide fuel cells – a review. Int J Hydrogen Energy 2019;44:7448–93. https://doi.org/10.1016/j.ijhydene.2019.01.212.
[16] K41 technical data sheet. ArcelorMittal; n.d.
[17] Meier GH, Jung K, Mu N, Yanar NM, Pettit FS, Abellán JP, et al. Effect of alloy composition and exposure conditions on the selective oxidation behavior of ferritic Fe–Cr and Fe–Cr–X alloys. Oxid Met 2010;74:319–40. https://doi.org/10.1007/s11085-010-9215-5.
[18] Talic B, Falk-Windisch H, Venkatachalam V, Hendriksen PV, Wiik K, Lein HL. Effect of coating density on oxidation resistance and Cr vaporization from solid oxide fuel cell interconnects. J Power Sources 2017;354:57–67. https://doi.org/10.1016/j.jpowsour.2017.04.023.
[19] Chandra-Ambhorn S, Wouters Y, Antoni L, Toscan F, Galerie A. Adhesion of oxide scales grown on ferritic stainless steels in solid oxide fuel cells temperature and atmosphere conditions. J Power Sources 2007;171:688–95. https://doi.org/10.1016/j.jpowsour.2007.06.058.
[20] Bianco M, Tallgren J, Hong J-E, Yang S, Himanen O, Mikkola J, et al. Ex-situ experimental benchmarking of solid oxide fuel cell metal interconnects. J Power Sources 2019;437. https://doi.org/10.1016/j.jpowsour.2019.226900. 226900.
[21] Kuhn B, Jimenez CA, Niewolak L, Hüttel T, Beck T, Hattendorf H, et al. Effect of Laves phase strengthening on the mechanical properties of high Cr ferritic steels for solid oxide fuel cell interconnect application. Mater Sci Eng A 2011;528:5888–99. https://doi.org/10.1016/j.msea.2011.03.112.
[22] Li J, Zhang W, Yang J, Yan D, Pu J, Chi B, et al. Oxidation behavior of metallic interconnect in solid oxide fuel cell stack. J Power Sources 2017;353:195–201. https://doi.org/10.1016/j.jpowsour.2017.03.092.
[23] Wang K, Liu Y, Fergus JW. Interactions between SOFC interconnect coating materials and chromia. J Am Ceram Soc 2011;94:4490–5. https://doi.org/10.1111/j.1551-2916.2011.04749.x.
[24] Tallgren J, Bianco M, Mikkola J, Himanen O, Rautanen M, Kiviaho J, et al. Comparison of different manganese-cobalt-iron spinel protective coating for SOFC interconnects. XII European SOFC & SOE Forum; 2016. p. 114–24.
[25] Haanappel VAC, Shemet V, Gross SM, Koppitz Th, Menzler NH, Zahid M, et al. Behaviour of various glass–ceramic sealants with ferritic steels under simulated SOFC stack conditions. J Power Sources 2005;150:86–100. https://doi.org/10.1016/j.jpowsour.2005.02.015.
[26] Evans HE, Donaldson AT, Gilmour TC. Mechanisms of breakaway oxidation and application to a chromia-forming steel. Oxid Met 1999;52:379–402. https://doi.org/10.1023/A:1018855914737.
[27] Othman NK, Zhang J, Young DJ. Water vapour effects on Fe–Cr alloy oxidation. Oxid Met 2010;73:337–52. https://doi.org/10.1007/s11085-009-9183-9.
[28] Wagner C. Theoretical analysis of the diffusion processes determining the oxidation rate of alloys. J Electrochem Soc 1952;99:369–80. https://doi.org/10.1149/1.2779605.
[29] Bowen AW, Leak GM. Diffusion in Bcc iron base alloys. Metall Trans 1970;1:2767–73. https://doi.org/10.1007/BF03037813.
[30] Yokokawa H, Horita T, Sakai N, Yamaji K, Brito ME, Xiong Y-P, et al. Thermodynamic considerations on Cr poisoning in SOFC cathodes. Solid State Ion 2006;177:3193–8. https://doi.org/10.1016/j.ssi.2006.07.055.
[31] Liu W, Konysheva EY. Conductivity of SrCrO4 and its influence on deterioration of electrochemical performance of cathodes in solid oxide fuel cells. ECS Trans 2014;59:327–32. https://doi.org/10.1149/05901.0327ecst.
[32] Montero X, Tietz F, Sebold D, Buchkremer HP, Ringuede A, Cassir M, et al. MnCo1.9Fe0.1O4 spinel protection layer on commercial ferritic steels for interconnect applications in solid oxide fuel cells. J Power Sources 2008;184:172–9. https://doi.org/10.1016/j.jpowsour.2008.05.081.
[33] Yu Y, Ludwig KF, Woicik JC, Gopalan S, Pal UB, Kaspar TC, et al. Effect of Sr content and strain on Sr surface segregation of La1–xSrxCo0.2Fe0.8O3–δ as cathode material for solid oxide fuel cells. ACS Appl Mater Interfaces 2016;8:26704–11. https://doi.org/10.1021/acsami.6b07118.
[34] Chen L, Magdefrau N, Sun E, Yamanis J, Frame D, Burila C. Strontium transport and conductivity of Mn1.5Co1.5O4 coated Haynes 230 and Crofer 22 APU under simulated solid oxide fuel cell condition. Solid State Ion 2011;204–205:111–9. https://doi.org/10.1016/j.ssi.2011.10.004.
[35] Bianco M, et al. [unpublished results n.d].

[36] Kim H, Seo D-H, Kim H, Park I, Hong J, Park K-Y, et al. Multicomponent effects on the crystal structures and electrochemical properties of spinel-structured M3O4 (M = Fe, Mn, Co) anodes in lithium rechargeable batteries. Chem Mater 2012;24:720–5. https://doi.org/10.1021/cm2036794.
[37] Morin F, Beranger G, Lacombe P. Limits of application for Wagner's oxidation theory. Oxid Met 1972;4:51–62. https://doi.org/10.1007/BF00612507.
[38] Gavrilov NV, Ivanov VV, Kamenetskikh AS, Nikonov AV. Investigations of Mn–Co–O and Mn–Co–Y–O coatings deposited by the magnetron sputtering on ferritic stainless steels. Surf Coat Technol 2011;206:1252–8. https://doi.org/10.1016/j.surfcoat.2011.08.036.
[39] Zhang HH, Zeng CL. Preparation and performances of Co–Mn spinel coating on a ferritic stainless steel interconnect material for solid oxide fuel cell application. J Power Sources 2014;252:122–9. https://doi.org/10.1016/j.jpowsour.2013.12.007.
[40] Rufner J, Gannon P, White P, Deibert M, Teintze S, Smith R, et al. Oxidation behavior of stainless steel 430 and 441 at 800°C in single (air/air) and dual atmosphere (air/hydrogen) exposures. Int J Hydrogen Energy 2008;33:1392–8. https://doi.org/10.1016/j.ijhydene.2007.12.067.
[41] Amendola R, Gannon P, Ellingwood B, Hoyt K, Piccardo P, Genocchio P. Oxidation behavior of coated and preoxidized ferritic steel in single and dual atmosphere exposures at 800°C. Surf Coat Technol 2012;206:2173–80. https://doi.org/10.1016/j.surfcoat.2011.09.054.
[42] Tveten B, Hultquist G, Norby T. Hydrogen in chromium: influence on the high-temperature oxidation kinetics in O2, oxide-growth mechanisms, and scale Adherence. Oxid Met 1999;51:221–33. https://doi.org/10.1023/A:1018866505708.
[43] Jablonski PD, Cowen CJ, Sears JS. Exploration of alloy 441 chemistry for solid oxide fuel cell interconnect application. J Power Sources 2010;195:813–20. https://doi.org/10.1016/j.jpowsour.2009.08.023.
[44] Barnes JJ, Goedjen JG, Shores DA. A Model for stress generation and relief in oxide — metal systems during a temperature change. Oxid Met 1989;32:449–69. https://doi.org/10.1007/BF00665449.
[45] Liu WN, Sun X, Stephens E, Khaleel MA. Life prediction of coated and uncoated metallic interconnect for solid oxide fuel cell applications. J Power Sources 2009;189:1044–50. https://doi.org/10.1016/j.jpowsour.2008.12.143.
[46] Menzler NH, Batfalsky P, Beez A, Blum L, Gross-Barsnick S. Post-test analysis of a solid oxide fuel cell stack operated for 35000 h. In: XII EFCF proc, A11. Luzern; 2016.